Engineering Computations

Estimating 3D particle motion from high-speed video for simulation validation
Mathew Price Garry Morrison

Article information:

For Authors

About Emerald www.emeraldinsight.com

Estimating 3D particle motion from high-speed video for simulation validation

Mathew Price

Cogency, Cape Town, South Africa, and

Garry Morrison

DebTech, De Beers Group Services, Johannesburg, South Africa

Abstract

Purpose – The purpose of this paper is to present an image based method for estimating the 3D motion of rigid particles from high-speed video footage (HSV). The computed motion can be used as either a means to generate quantitative feedback for a process or to validate the accuracy of discrete element method (DEM) simulation models.

Design/methodology/approach – Experiments consist of a diamond impacting an angled plate and video is captured at 4,000 frames per second. Simple image analysis is used to track the particle in each frame and to extract its 2D silhouette boundary. Using an approximate 3D model of the particle generated from a multi-camera setup, a pose estimation scheme based on silhouette consistency is used in conjunction with a rigid body model to compute the 3D motion.

Findings – Under reasonable conditions, the method can reliably estimate the linear and angular motion of the particle to within 1 per cent of their true values.

Practical implications – As an example application, we demonstrate how the method can be used to validate DEM simulations of simple impact experiments captured with HSV, providing valuable insight towards further development. In particular, we investigate the effects of shape representation through sphere-clumping and the applicability of different contact models.

Originality/value – The novelty of our method is its ability to accurately compute the motion associated with a real world interaction, such as an impact, which provides numerical ground truth at an individual particle level. While similar schemes have been attempted with ideal particles (e.g. spheres), the resulting models do not naturally extend to realistic particle shapes. Since our method can track real particles, real-world processes can be better quantified.

Keywords Particle size measurement, Motion, Video

Paper type Research paper

1. Introduction

Understanding mass particle interaction in large scale processes is a complex problem. Discrete element methods (DEM) are widely used in particle-based analysis for determining the dynamic motion of a large number of particles in various processes by means of simulation. Emergent behaviour of the system is sought by simulating a large number of individual particles which interact according to specified mechanisms. These mechanisms operate at a single particle level. Hence, incorporation of appropriate particle shape representations and interaction models is important for successful simulation.

Particle dynamics simulation generally results in a vast simplification of the real-world process in order to extract a computationally viable model. Various proposals have been made to circumvent problems caused by these simplifications. In the case of shape representation, these include sphere clumping and superquadric representations (Williams, 1991) as improvements over the typical representation of particles as spheres. However, such methods, while possibly improving accuracy, come at the price of an increased computational overhead. Empirical spring and dashpot contact models

are often employed to capture a degree of the inelastic material response (Walton and Braun, 1986). While such models have the advantage of speed, they do not relate to material properties, making them difficult to generalise. Although some progress has been made in the development of phenomenological contact models that are parameterised by relevant material properties (Li *et al.*, 2002), these are often computationally expensive.

The importance of improved shape representation is increasingly being recognised. Of course, shape representation and the choice of a suitable contact model are interconnected because the material response of the contacting bodies may differ depending on the contact geometry. The material response to particle contacts can range from elastic to elasto-plastic to plastic. The shortcomings of using linear spring or Hertz contact models in conjunction with the spherical particle approximation may be more obvious in sparse systems, characterised by a long mean-free-path between collisions. However, they can be equally limiting in dense-packed systems where mechanical interlocking of particles is prevalent.

Validation is an important component of simulation-based design. The validation needs to occur at both a global and a mechanism level. In multi-particle processing systems, detailed global validation can be difficult because tracking and measurement of individual particles is intractable. Hence, one form of global validation involves comparing gross trends such as particle throughput, density and power draw. Validation of single particle interaction mechanisms can be no less problematic, even in the case of simple shapes, such as spheres. In this paper we discuss the development of a method that can be used to assist in the validation of single particle contact models involving real particle shapes.

A pre-requisite for our method is an accurate 3D model of the tracked particle. This information is used to track the motion of the particle in a high-speed video (HSV) sequence captured with a single camera. After a discussion of how the motion estimation method works, we will present the results of our application of the method to the analysis of a number of particle impacts on an angled plate. Our limited application of the developed technique demonstrates its use as a method for validating the suitability of the contact model and shape representation employed at a single particle level.

2. Motion estimation framework

Given a HSV sequence of a particle impacting a plate, the objective is to determine the 3D motion associated with the particle. This involves computing the position and orientation, or *pose*, of the particle in each image of the sequence. From this information, the trajectory can be reconstructed and used to initialise a simulated version of the experiment. Since the reconstructed trajectory corresponds to particle motion in the real world, it can be used to gauge the accuracy of the simulated experiment if suitable material properties for the contacting bodies are known.

Assuming the particle undergoes unhindered rigid body motion both before and after impact, the full trajectory can be modelled as a train of piecewise trajectories separated by collision events. This simplifies the motion estimation problem, since each piecewise component corresponds to a constant linear and angular momentum term. Constant forces, such as gravity, can also be included in the model with minimal additional complexity. Currently, we do not consider cases in which the particle rolls along the plate.

2.1 Particle shape

The angular component of a particle's motion is dependent on its shape. Therefore, the 3D shape of a particle must be determined beforehand. In our work, a shape-from-silhouette approach is used whereby an approximate 3D model of a particle is generated using a separate six-camera setup (Figure 1). The cameras are calibrated, i.e. the relative poses are known and the silhouette boundaries of the particle are extracted from each image. The combination of silhouettes and their corresponding camera calibration parameters is referred to as a *silhouette set*.

The intersection of the visual cones formed from a silhouette set is known as the *visual hull* (Laurentini, 1994). This is the largest shape that could have generated the silhouettes and forms an upper bound on the volume of the particle. Since a six-view visual hull provides a relatively coarse shape approximation, we merge multiple six-view silhouette sets of a particle to form more accurate shape models (Forbes *et al.*, 2003). In our application, ten runs for each particle are captured resulting in 60-view silhouette sets (i.e. the particle is effectively seen from 60 different viewpoints).

2.2 Pose estimation

A particle is moving with respect to a fixed camera whose relative pose is unknown. Equivalently, if we consider the particle to be static, the problem can be visualised as someone attempting to move the camera around the particle so that a projection of the particle into the camera view corresponds to the image seen by the camera.

The relative pose between the world and the reference frame of a camera is specified by a rigid transform P_{wc} with a homogenous coordinate system:

$$P_{wc} = \begin{bmatrix} R & \mathbf{t} \\ 0 & 1 \end{bmatrix}, \tag{1}$$

where R is a 3×3 rotation matrix and $\mathbf{t}$ is a 3×1 vector corresponding to a translation. Therefore, the pose estimation problem corresponds to finding appropriate values for R and $\mathbf{t}$. Figure 1 illustrates this scenario.

Figure 1.
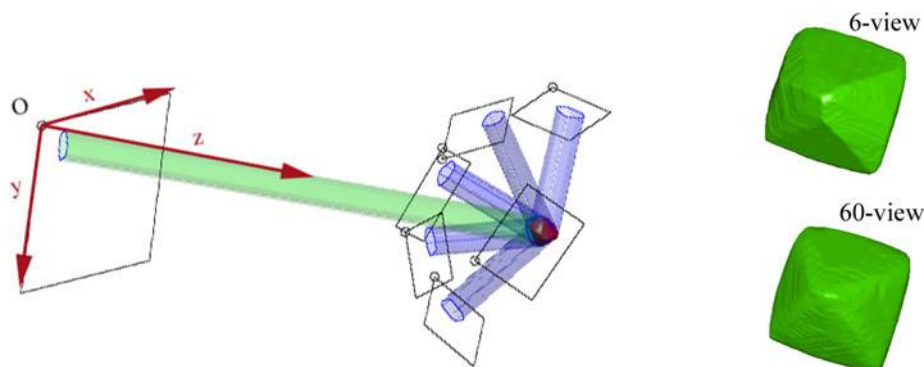
Notes: The 3D model of the particle (visual full) is the result of the intersection of all the visual cones; the unknown viewpoint associated with the a particle's pose in HSV sequence is shown with respect to the calibrated silhouette set on the left; left: a typical six-view calibrated silhouette set associated with the six camera setup; right: example of a six- and 60-view visual hull

P_{wc} is estimated from silhouettes by maximising the silhouette consistency between the unknown camera and the calibrated silhouette set. A convenient measure of silhouette consistency is the epipolar tangency error (ETE), which measures the extent to which the visual cones, formed by rays passing through a camera centre and a corresponding silhouette boundary, correctly intersect. The primary advantage of this formulation is its efficiency, since it can be computed directly from a silhouette set and does not require an explicit 3D model (e.g. polygonised mesh). In addition, since the measure is based on a geometric constraint, it can be formulated as an objective function that can be minimised using standard non-linear least-squares optimisation.

2.3 The ETE
Consider two views of an object as shown in the left of Figure 2. Each camera (C_A and C_B) images an object from different views resulting in the corresponding silhouettes S_A and S_B. We assume a pinhole camera model, thus the visual cones of the silhouettes converge to the camera centres c_a and c_b.

The projection of a camera centre into another camera's image plane is called an *epipole*. Epipoles are points of intersection of the line created by joining two camera centres (the baseline) and the respective image planes. In the figure, epipoles e_{aB} and e_{bA} corresponding to the projections of c_a and c_b into cameras C_B and C_A, respectively are shown. Epipolar tangency lines are constructed for each view by drawing lines from the epipoles to their corresponding silhouette boundary in each image, such that they graze their silhouettes. The epipolar tangency lines, which exist in 2D image space, touch their silhouettes at the epipolar tangency points (t_{a1}, t_{a2}) for S_A and (t_{b_1}, t_{b_2}) for S_B. Since these points are projections of the same 3D points, called *frontier* points, they must be consistent across both views. That is, the ray passing through c_a and t_{a_1} must project exactly onto the epipolar tangency line $e_{aB}t_{b1}$. This is known as the epipolar tangency constraint (Wong, 2001). In practice, there is inherent noise in the imaging process and the camera parameters are not without error, which leads to inexact projection of the epipolar tangency lines as illustrated in Figure 2, right.

The perpendicular distance between an epipolar tangency point and a projected epipolar tangency line from another view is called the ETE. The ETE is measured in pixels and provides a convenient measure of inconsistency between two silhouette projections. For each pair of silhouettes there are two epipolar tangency points for each image, resulting in four ETE's. A detailed explanation on computing the ETE can be found in Forbes *et al.* (2003).

3. 3D trajectory estimation
Estimating the pose of a particle for an entire sequence typically requires estimating a rigid transform (Equation (1)) for each frame. Our method simplifies this by using a
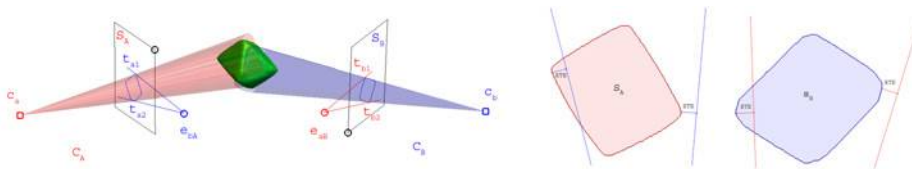
Notes: Left: An object viewed from two cameras with corresponding epipoles and epipolar tangents shown; right: example illustrating epipolar tangency error (ETE)

Figure 2.

rigid body motion model to predict the pose of the particle during frames in which the particle is moving unhindered, i.e. not colliding with any other body and not subjected to dynamic force fields. After estimating the pose of the particle for the first frame, the camera parameters for the remaining frames are generated by simulating the particle according to the motion model parameters. The ETE is retained as a measure of how inconsistent the resulting trajectory is with respect to the calibrated silhouette set of the particle. This results in a pose estimation framework that makes use of the silhouette consistency constraint while ensuring that only physically possible solutions are found. We assume that the particle is considered to be a rigid body, and that particle motion between impact events follows unhindered rigid body motion.

3.1 Particle initialisation
The first task in determining the trajectory of a particle in a HSV sequence is to estimate its initial pose. The formulation discussed in section 2.2 is used. Given the particle's silhouette at the beginning of the HSV sequence (unknown camera) and a calibrated silhouette set of the particle (six-camera setup), we wish to determine the relative pose of the unknown camera. This is illustrated in Figure 1.

A perspective camera model with square pixels and no lens distortion is assumed for the unknown camera, which is specified by a 4×4 projection matrix P:

$$K = \begin{pmatrix} f & 0 & u_x \\ 0 & f & u_y \\ 0 & 0 & 1 \end{pmatrix} \tag{2}$$

$$P = \begin{bmatrix} K & 0 \\ 0 & 1 \end{bmatrix} \begin{bmatrix} R & t \\ 0 & 1 \end{bmatrix}. \tag{3}$$

K contains the camera's intrinsic parameters, focal length f and principal point (u_x, u_y) and is used to define the perspective projection. R and t form a rigid body transform that orients the world to the camera's reference frame. A convenient parameterisation for rotations is to use quaternions, which provides a more compact representation. A unit quaternion $\mathbf{Q}$ is specified by four parameters and is associated with a unique orientation. Another reasonable assumption is that the principal point (the projection of the camera centre onto the image plane) is approximately at the centre of the image. The unknown camera can therefore be specified by eight parameters:

$$\mathbf{X} = [\mathbf{f} \quad \mathbf{Q}^T \quad \mathbf{t}^T], \tag{4}$$

where $\mathbf{X}$ represents a concatenated vector of parameters.

Suitable parameter values can be efficiently determined by iterative non-linear least-squares optimisation – here the Levenberg-Marquardt method (Moré, 1977) is used (LM optimisation). The objective function for the optimisation is specified by a concatenated vector of ETE's, which are formed by considering all forward and reverse pairings between the unknown silhouette and each silhouette view in the calibrated set. This leads to $4n$ errors (from $2n$ pairs), where n is the number of silhouettes in the calibrated silhouette set.

3.2 Motion parameters
After determining the initial pose of the particle, the trajectory can be estimated by finding rigid body motion parameters that best reproduce the particle's motion in the HSV sequence. Each sequence is associated with an uncalibrated silhouette set, i.e. there is an unknown view of the particle for each frame in the sequence. We define the particle state by the vector

$$\mathbf{Y}(t) = \begin{bmatrix} \mathbf{x}(t)^{\mathrm{T}} & \mathbf{Q}(t)^{\mathrm{T}} & \mathbf{P}(t)^{\mathrm{T}} & \mathbf{L}(t)^{\mathrm{T}} \end{bmatrix}, \tag{5}$$

relating to position, orientation (quaternion representation), linear momentum and angular momentum, respectively.

Under the assumption of unhindered rigid body motion, if we know $\mathbf{Y}(t_0)$ then all future states (until a collision) can be determined. From the initial pose estimation (section 3.1), $\mathbf{x}(t_0)$ and $\mathbf{Q}(t_0)$ are already known. Therefore, we need to determine suitable values for the linear and angular momentum terms. As before the LM optimisation is used. The parameter vector for optimisation is

$$\mathbf{Z} = [\mathbf{P}(t_0)^{\mathrm{T}} \quad \mathbf{L}(t_0)^{\mathrm{T}}]. \tag{6}$$

Next, an objective error function must be defined. With any given parameter vector $\mathbf{Z}$, we associate a set of simulated states $\beta = \{\mathbf{Y}(t_0) \dots \mathbf{Y}(t_{n-1})\}$, where n is the number of frames in the sequence. Since the derivative of the state vector is

$$\frac{d}{dt}\mathbf{Y}(t) = \begin{bmatrix} \mathbf{v}(t)^{\mathrm{T}} & \frac{1}{2}\boldsymbol{\omega}(t)\mathbf{Q}(t)^{\mathrm{T}} & \mathbf{F}(t)^{\mathrm{T}} & \boldsymbol{\tau}(t)^{\mathrm{T}} \end{bmatrix}, \tag{7}$$

$(\mathbf{v}, \boldsymbol{\omega}, \mathbf{F}$ and $\boldsymbol{\tau}$ are linear velocity, angular velocity, force and torque) β can be determined using a standard ODE solver. In our implementation we have found that a fourth order Runge-Kutta solver produces good results (Eberly, 1999).

To retain the ETE as the measure of silhouette consistency for the optimiser's objective function, the set of state vectors β must be converted to an equivalent set of camera projection matrices $\Psi = \{P_1 \dots P_n\}$. Similarly, we define Ω as the set of projection matrices corresponding to the calibrated silhouette set of the particle (i.e. from the six-camera setup). This representation may require a transformation if the simulation's reference frame differs from that of the camera. For simplicity, we use the conventional camera reference frame, depicted in Figure 1, for both systems. Having identical reference frames leads to the following direct relation between a state vector $\mathbf{Y}(t_i)$ and a corresponding camera projection matrix P_{i+1}:

$$P_{i+1} = \begin{bmatrix} \mathrm{K} & 0 \\ 0 & 1 \end{bmatrix} \begin{bmatrix} \mathrm{R}(t_i) & \mathbf{x}(t_i) \\ 0 & 1 \end{bmatrix}, \tag{8}$$

where $\mathrm{R}(t_i)$ is the rotation matrix corresponding to $\mathbf{Q}(t_i), 0 \leq i < n - 1$ and K is the constant matrix of intrinsic camera parameters from Equation (2). If $S = \{S_1 \dots S_n\}$ is the set of silhouettes associated with the set of projection matrices Ψ, then let $\{S, \Psi\}$ denote the silhouette set corresponding to the uncalibrated HSV sequence. Similarly, let $\{C, \Omega\}$, with $C = \{C_1 \dots C_m\}$, be the calibrated silhouette set of the particle acquired from the six-camera setup. The silhouette consistency across both silhouette sets can therefore be computed by pairing each silhouette from $\{S, \Psi\}$ with each silhouette in

$\{C, \Omega\}$ and vice versa, resulting in nm pairings and thus $4nm$ ETE's. The concatenation of these errors forms the objective function used by the LM optimisation. Final refinement of the solution is conducted by adding inter-silhouette pairings within $\{S, \Psi\}$. This enables the uncalibrated silhouette set to be optimised for internal as well as external consistency.

664

3.3 Piecewise trajectories

The above procedure is extended by introducing the notion of piecewise rigid body motion, so that motion across impact frames is handled transparently. In simple interactions, sets of frames relating to unconstrained rigid body motion can be separated by a set of collision events. Therefore, the sequence can be described as a piecewise combination of rigid body trajectories that are separated by a set of discontinuous impulses. The advantage of this formulation is that the complexities of mechanical interaction during contact can be bypassed by treating their combination as a unified event, which results in the instantaneous change of momentum. From the point of view of the particle, there are two separate rigid body trajectories, which overlap at some time and hence share a common pose as illustrated in Figure 3.

Since the contact duration is substantially less than the inter-frame time, the exact collision time does not occur at any particular frame, but rather between frames. As we are estimating the motion of the particle so that it replicates an imaged experiment, discrete time steps are enforced. Given a set of silhouettes as input, the angles between successive centroids is used to automatically divide the set into piecewise rigid body trajectories. After estimating the parameters for the first piecewise trajectory, the impact frame is automatically determined by intersecting a simulation of the first piecewise trajectory with an approximation of the second piecewise trajectory. The approximate trajectory is formed by fitting a second order polynomial curve to the 2D centroids of the corresponding silhouettes (shown in Figure 3). If $S1 = \{S_1 \ldots S_\alpha\}$ and $S2 = \{S_\alpha \ldots S_n\}$ are sets of silhouettes corresponding to the first and second piecewise trajectories respectively, then the generalised 3D trajectory estimation method is as follows:

(1) Estimate Ψ_1 for $S1$ using the trajectory estimation method (from sections 3.1 and 3.2).

(2) Approximate collision frame α using newly estimated trajectory (Figure 3).

(3) Estimate Ψ_2 for $S2$ using projection matrix P_α from Ψ_1 as the initial pose.

(4) Refine global solution $\{S1, \Psi_1\} \bigcup \{S2, \Psi_2\}$ for maximum silhouette consistency.

3.4 Initial parameter selection

A common issue with optimisation frameworks is their sensitivity to the initial parameters. It is possible for the optimisation to become trapped in local minima,

Figure 3.
Piecewise trajectory splitting for a particle impacting a plate (left) with automatic collision frame detection (right)
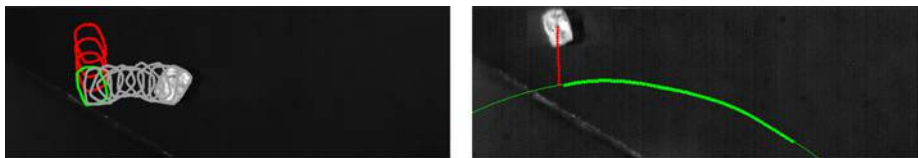
which results in the camera parameters being unable to move towards the correct solution without increasing the residual error term. This occurs often with more regularly shaped particles since several possible poses can be equally consistent. One workaround is to apply multiple optimisations with different starting points. In particular, the primary cause of locking in the initial pose estimation process is the choice of the camera's initial orientation. This problem is alleviated by repeatedly sampling random orientations (quaternions) from a normal distribution. The search can be terminated by setting a suitable threshold on the RMS value of the ETE vector (e.g. 1 pixel).

In the case of estimating the motion parameters, the equivalent problem is encountered with the initial choice of angular momentum $\mathbf{L}(t)$. Here random angular momentum directions (3×1 vectors) are sampled from a normal distribution and the magnitude of the vector is limited so that exceptionally large momentum values that cause numerical instability are avoided.

4. Experiments and results

Results are divided into two groups. In the first, we use synthetic data to evaluate our method in terms of how well the initial pose and trajectory estimation techniques perform under various conditions.

The second group of results corresponds to experiments based on real data where the method is applied to HSV drop tests involving a particle and an angled plate. The initial conditions provided by the method are used to generate simulated DEM versions of the real event that can be used for validation. The ability to compare a simulated particle impact to one that occurs in reality offers valuable insight into the predictive accuracy of DEM methods. As an example, we show comparative results for particle velocity under different contact models and shape representations.

Since actual ground truth is not available for these validation experiments, we use the overall RMS ETE as an indicator that an acceptable solution has been found. A low overall ETE implies that the calibration between the silhouettes in a HSV sequence and those forming the original multi-view particle model is consistent, i.e. there is a good fit between the estimated trajectory and the physically permissable trajectory.

4.1 Method evaluation

The extent to which the full motion of a particle can be estimated is largely related to the success of the estimation of the initial pose. In this section we first discuss the effectiveness of the particle initialisation process (section 3.1). This is followed by an evaluation of the motion estimation process (section 3.2), in which synthetic sequences generated from real particles are used to provide ground truth.

4.1.1 Particle initialisation. Using a 60-view silhouette set of a known particle, a leave-one-out validation scheme is used in which each silhouette is removed from the set in turn and its pose is estimated. The estimated pose is then compared with the silhouette's original calibrated pose, which is deemed to serve as ground truth. Figure 4 shows the results for three runs of six particles (using different starting points), where three particles are regular in shape and three are irregular. This results in three pose estimates for each silhouette from a 60-view set and a total of 540 pose estimates for both regular and irregular particles. Errors are binned according to the angular orientation error. From the distributions it is evident that single view poses from irregular particles are more consistently estimated than for regular particles. The small peaks located near the 180° bin show cases where the antipodal view has been found
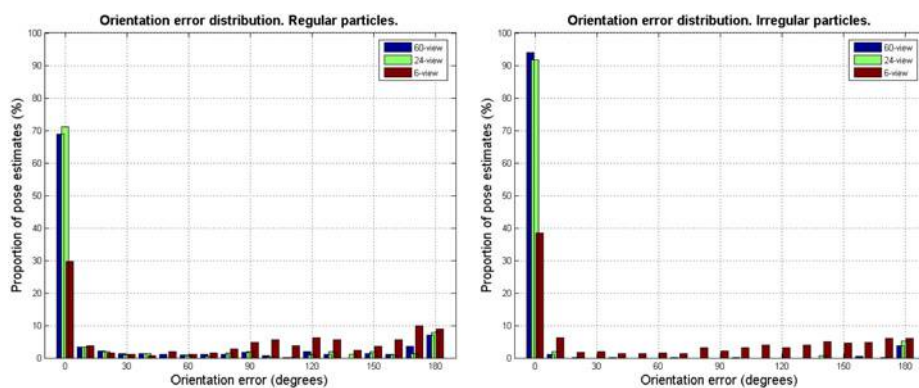
Figure 4.
Orientation error
distributions

Notes: Left: regular particles (66 per cent of the estimates are accurate to within 5°);
right: irregular particles (88 per cent of the estimates are accurate to within 5°); each
bin represents 10°

instead. This occurs because random orientations close to the antipodal view may
appear similar and therefore result in a local minimum in the ETE function.
Experiments conducted with smaller silhouette sets (six- and 24-view) show that the
reliability of the solution degrades gracefully with decreasing number of views.

4.1.2 Trajectory estimation. The accuracy of the trajectory estimation method is
measured from synthetic data. Non-contacting simulated trajectories of randomly
selected particles are randomly generated and our method is used to estimate the linear
and angular components of the motion. Simulations were conducted in which the
sequence length, linear momentum and angular momentum were randomly varied. In
addition, particles were initialised to views from their calibrated silhouette sets, thus
particle initialisation does not contribute any error in these results. Although the
silhouettes extracted from the simulated trajectory are synthetic, the estimation uses
the particle's original calibrated silhouette set, which corresponds to real data.
Therefore, these tests provide a realistic means of assessing our method given that the
image segmentation in the HSV sequence is ideal. Figure 5 summarises the results,
which are based upon the linear and angular velocity errors.

In Figure 5, the component velocity errors relative to the cameras' reference frames
are shown. In-plane velocities correspond to x and y values, while z represents out-of-
plane velocities. Two dominant effects can be seen: the linear velocity estimation
improves as the sequence length increases (top, left plot) and the angular velocity
estimation improves as the ETE decreases (top, right plot).

Interestingly, even though we only make use of one high-speed camera, out-of-plane
linear velocity can still be reasonably estimated when the sequence is long enough.
Naturally, this will depend on the ratio between the actual particle velocity and the
frame rate of the HSV camera. In our simulations a fixed frame rate of 4,000 fps was
used and particle velocity varied between zero and four m/s.

The top, right plot shows that a low ETE corresponds to a lower error in estimation
of the angular velocity. Additionally, the existence of the second cluster on the right
hand side of the top, right plot illustrates cases in which insufficient angular
momentum starting points were used. In our simulations, a maximum of 100 starting
points was used. Therefore, greater overall consistency may be achieved by only
accepting solutions once the ETE is below a specified threshold.

Figure 5.
Linear and angular
velocity estimation error
for 1,200 simulated
trajectories.
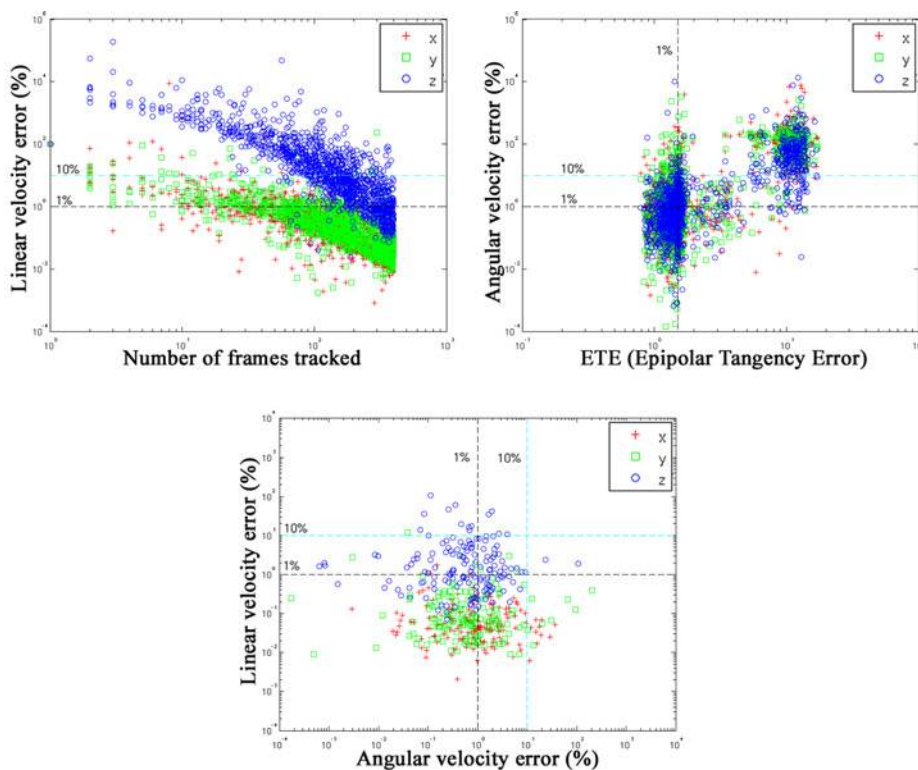
Notes: Lower plot shows comparative linear and angular velocity errors for simulations where the sequence length is greater than 100 and the ETE is below 1.5 pixels

The previous results indicate that if the sequence is reasonably long, the particle shape is irregular and segmentation is accurate, then in most cases the linear and angular velocities of the particle can be estimated to within 1 and 10 per cent, respectively (bottom plot).

4.2 Validation experiments

One application for our trajectory estimation method involves the validation of contact and shape models used in DEM simulators. Typically, this type of validation has been accomplished using analysis of sphere impacts, since Hertzian type models are often used and accurate tracking of more complicated particle shapes is problematic. Here we show how validation can be achieved for realistic particle shapes, thereby enabling a closer comparison between the predicted motion of a particle within a simulation and a real world interaction.

Four HSV experiments consisting of irregular diamond particles impacting an angled, hardened steel plate (Vickers Hardness 750 kg/mm^2) are used for our validation experiments. A particle dropper is used to ensure that the particle is consistently dropped from a known height, allowing the pre-impact velocity to be verified. This was confirmed to be approximately 2.21 m/s, which is roughly three times greater than the estimated yield velocity of 0.71 m/s, below which no plastic deformation occurs. The corresponding velocity ratio results in an estimated normal

coefficient of restitution of approximately 0.95 (Li *et al.*, 2002). Thus no significant plastic deformation is expected. Sixty-view calibrated silhouette sets of the particle are used for the registration process. Motion estimation is applied and the solution is accepted when the overall ETE falls below 1.5 pixels.

4.2.1 Sphere clump experiments. Typically, DEM simulations are computationally intensive due to the high number of particles that are simulated. For this reason, particles are often approximated by spheres since it simplifies collision detection and enables the use of Hertzian contact models, which is well understood. Towards providing support for more realistic shape representations, certain DEM codes allow the specification of clumped elements (Itasca Consulting Group Inc., 2006; DEM Solutions, 2006). In this formulation groups of overlapping primitives (typically spheres) are used to more accurately approximate the desired shape.

In this section, we investigate the effectiveness of sphere clump modelling for simulation. In particular, we explore how the number of spheres affects the accuracy of the simulation. Sphere clumps are generated using an automatic method (Price *et al.*, 2007) that seeks to optimise the surface correspondence between the sphere clump and a triangular mesh of the particle. We consider good shape representation to be attained when the volumes, centroids and second order moments are similar between the sphere clump and the original mesh of the particle. Figure 6 shows some images of rendered sphere clumps generated from 3D meshes of real diamonds.

Sphere clumps of variable numbers of spheres were generated and used to represent the particle within the simulations (rightmost particle in Figure 6). For each experiment the DEM simulation was initialised according to the initial particle conditions at the beginning of the HSV sequence. Figure 7 shows the post-impact linear and angular velocity error for each test. Results are shown for both the standard Hertz contact (Johnson, 1985) and the no-slip Hertz-Mindlin contact (Di Renzo and Di Maio, 2004),

Figure 6.
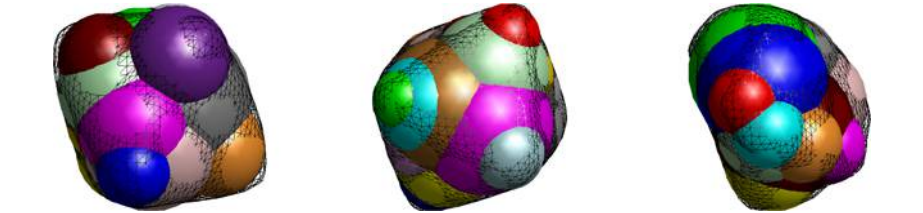Example sphere clumps generated from 3D meshes of real diamonds
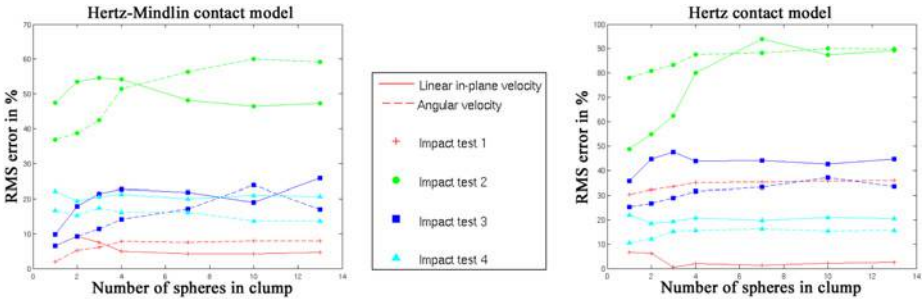

Figure 7.
Linear and angular post-impact velocity error for several HSV tests versus the number of spheres in the clump

Notes: Left: DEM with Hertz-Mindlin (no-slip) contact model. Right: DEM with Hertz contact model
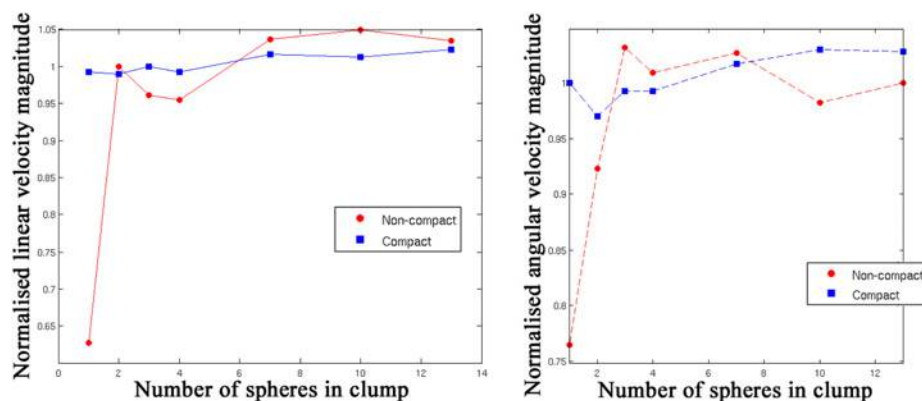
which appears in several commercial DEM codes. For the linear velocities, only the in-plane component (parallel to the HSV image plane) is used. This is because out-of-plane linear motion estimation may be unreliable when only one HSV camera is used (as discussed in the previous section).

Intuitively, one would expect simulations with a high number of spheres to achieve better accuracy. In particular, a notable variance in angular velocity would be expected between the single-sphere and multi-sphere cases. However, the results indicate that this is not the case for the experiments in question. This can be due to a number of reasons, including the accuracy of the sphere clump representation of the actual particle at the point of contact. In addition the degree of the plastic response of the plate will vary as a function of the local particle curvature at the point of contact. For a contact radius greater than the equivalent spherical particle the degree of the plastic response will be less, whilst for a relatively smaller contact radius the plastic response will be greater. This is not captured in the strictly elastic contact models we have employed.

It is interesting to note that better simulation accuracy is achieved through the use of an improved contact model (Hertz-Mindlin vs standard Hertz) than with improved shape representation with sphere clumps. This suggests that the Hertz-Mindlin contact model with slip, or better still, a contact model that more correctly captures the elasto-plastic nature of the contact will perform even better.

Another possible factor is that in our tests, although the particles shape is fairly irregular, it is also very compact. This leads to the centroid of the particle being located close to the centre of the sphere of equivalent volume. Therefore, the rotational moment, caused by the position of the contact point relative to the centroid at the moment of impact, is similar for both the single-sphere and multi-sphere configurations. This leads to similar torques and hence similar angular velocities. This is illustrated by the comparative simulation experiment shown in Figure 8. A non-compact particle was generated by extruding one of the real particles along an axis. The plots show how particle velocity variance between different sphere clump sizes is increased under simulation when the particle has a more irregular mass distribution.

In summary, the sphere clump representation performed surprisingly poorly compared to the single sphere in DEM simulations of a number particle-plate impacts. Since there was a degree of plastic deformation of the plate in our experiment, the possible causes of this anomaly include both our contact model and the shape

Figure 8.
Comparison of particle velocity variance for compact and non-compact particles in relation to the number of spheres in a clump

Notes: Velocities are normalised according to the median values overall results

representation as a sphere clump. In the future, we aim to repeat these experiments for a diamond impacting a polycrystalline diamond (PCD) plate. In this case the contact will be purely elastic, provided that no fracture of the plate or particle occurs. This will facilitate a more robust assessment of the value of a sphere clump representation of the particle.

4.2.2 Contact model experiments. The previous experiments showed that both particle shape and contact model play an important role in determining the accuracy of a simulation. Using sphere clumps composed of eight spheres, we now assess the accuracy of the contact model in a similar manner. In the previous experiments the no-slip Hertz-Mindlin contact model was shown to outperform the standard Hertz approach. Here we compare it to an ideal hard-sphere model. The particulars of the two contact models are as follows:

Hertz-Mindlin (no-slip) model: Building on Hertz theory, which provides solutions for the normal force-displacement under elastic spherical contact (soft-sphere model), Cattaneo-Mindlin-Deresiewicz Theory (Mindlin and Deresiewicz, 1953) presents a solution in the case of varying oblique forces. Using several simple loading scenarios, the tangential evolution of the contact point can be determined, resulting in improved contact modelling. In our simulations we use the simplified no-slip model as described in Di Renzo and Di Maio (2004), which typically appears in commercial DEM packages.

Impulse model: Based on the work of Mirtich (1996), this rigid body collision response model handles collisions of non-penetrating polyhedra by applying a series of impulses to the contacting bodies. This is sometimes referred to as the hard-sphere model, because material properties are not considered. Impulses are computed based on Stronge's hypothesis, which relates the normal work in the compression phase of the collision to the normal work in the restitution phase. This guarantees that the effects of the normal forces are purely dissipative, thereby ensuring that the addition of frictional components does not add energy to the system.

The motion estimation method was applied ten times to each of the sequences in order to verify whether consistent solutions are produced. While the majority of the motion estimates generated similar results, a few outliers were encountered. These were caused by degenerate cases in which the initial pose estimation was unsuccessful. Figure 9 summarises the results by comparing the DEM simulated particle velocities to those obtained from motion estimation of the respective HSV sequences. In terms of linear
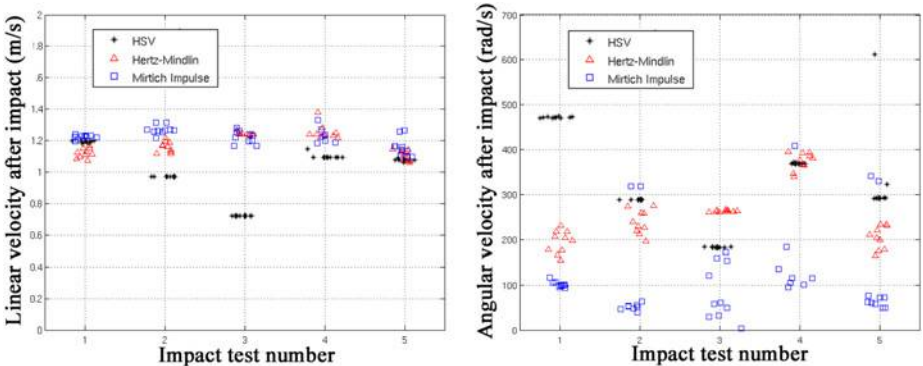
Figure 9.
Linear and angular velocities for simulations of five particle-plate HSV experiments

Notes: Ten runs of each experiment were processed in order to demonstrate repeatability; HSV markers correspond to velocities obtained from our registered trajectories; other markers correspond to velocity from simulations using Hertz-Mindlin and Mirtich impulse contact models

velocity, both models performed equally well. This is attributed to the material hardness of the contacting bodies and the low impact velocities, which minimises the effects of plasticity and justifies the use of a hard-sphere model. However, the Hertz-Mindlin model does appear to perform better in terms of angular velocity, and demonstrates more consistency. As mentioned in the previous section, expanding the experiments to include purely elastic contacts (i.e. diamond particles on PCD plates) will enable the effects of particle shape and contact model to be decoupled. This will promote a clearer understanding of the relative importance of these two components.

5. Conclusions and future work

A method for estimating the 3D motion of rigid particles from HSV experiments using a single camera is described. This enables quantitative feedback from real particle interactions, which can be used for process optimisation or simulation validation. In this paper a demonstrative example corresponding to comparative analysis of DEM shape and contact models has been shown.

The use of the epipolar tangency error provides an appropriate framework for pose estimation because it incorporates all geometric information available from the HSV images. Extensions such as texture analysis may aid estimation and boost consistency, but are unlikely to significantly improve results.

Synthetic testing has shown that the following factors affect the reliability of the method: the number of calibrated views available of particle, the amount of shape irregularity of the particle, the number of random starting points used for estimation, and the length of the HSV sequence.

Accurate estimation of out-of-plane velocities has proved difficult because only one HSV camera is used and consistency depends on the extent to which silhouette scale changes with such motion. Distant cameras corresponding to long focal lengths create near parallel viewing rays that impair the differentiation of motion along the viewing axis. Future experimentation will explore ways in which to cope with this problem, e.g. multi-camera setups.

In terms of applications, the method was used to validate DEM simulations of particle-plate drop tests. The simulation accuracy was evaluated both in terms of shape representation and contact model. Results confirm the strong interaction between shape and contact model under simulation, and the need for accurate modelling in each case. As expected, the Hertz-Mindlin formulation was shown to offer better accuracy over both the standard Hertz and ideal hard-sphere models. This is attributed to its incorporation of both tangential evolution of the contact point and the material properties of the contacting bodies.

References

DEM Solutions (2006), *EDEM v1.1 Manual*, DEM Solutions, Edinburgh.

Di Renzo, A. and Di Maio, F.P. (2004), "Comparison of contact-force models for the simulation of collisions in DEM based granular flow codes", *Chemical Engineering Science*, Vol. 59, pp. 525-41.

Eberly, D. (1999), "Numerical methods for ordinary differential equations", Technical report, Geometric Tools, available at: www.geometrictools.com

Forbes, K., Voigt, A. and Bodika, N. (2003), "Using silhouette consistency constraints to build 3D models", *Proceedings of the Fourteenth Annual South African Workshop on Pattern Recognition*.

672

Itasca Consulting Group Inc. (2006), *PFC3d Manual*.

Johnson, K.L. (1985), *Contact Mechanics*, Cambridge University Press, Cambridge, Chapter 4.

Laurentini, A. (1994), "The visual hull concept for silhouette-based image understanding", *IEEE Transactions on Pattern Analysis and Machine Intelligence*, Vol. 16 No. 2, pp. 150-62.

Li, L.Y., Wu, C.Y. and Thornton, C. (2002), "A theoretical model for the contact of elastoplastic bodies, Part C", *Journal of Mechanical Engineering Science*, Vol. 216, pp. 421-31.

Mindlin, R. and Deresiewicz, H. (1953), "Elastic spheres in contact under varying oblique forces", *ASME Journal of Applied Mechanics*, Vol. 20, pp. 327-44.

Mirtich, B.V. (1996), "Impulse-based dynamic simulation of rigid body systems", PhD thesis, University of California, Berkeley, CA.

Moré, J.J. (1977), "The Levenberg-Marquardt algorithm: implementation and theory", in Watson, G.A. (Ed.), *Lecture Notes in Mathematics*, Springer Verlag, Chapter "Numerical Analysis", pp. 105-16.

Price, M., Murariu, V. and Morrison, G.R. (2007), "Sphere clump generation and trajectory comparison for real particles", *Proceedings of the Discrete Element Methods 07*, available at: www.min-eng.com/ dem07/paps.html.

Walton, O.R. and Braun, R.L. (1986), "Viscosity, granular-temperature, and stress calculations for shearing assemblies of inelastic, friction discs", *Journal of Reology*, Vol. 30 No. 5, pp. 949-80.

Williams, J.R. (1991), "Superquadrics and model dynamics for discrete elements in concurrent design", Technical report IESL 91-12, Intelligent Engineering Systems Laboratory, Massachusetts Institute of Technology, Cambridge, MA.

Wong, K.-Y.K. (2001), "Structure and motion from silhouettes", PhD thesis, University of Cambridge, Cambridge.

About the authors

Mathew Price obtained a Masters degree in Electrical Engineering from the University of Cape Town (UCT) in 2004. He then continued on as a researcher at UCT in the field of Computer Vision, pursuing the development of 3D imaging and pattern recognition methods. He recently co-founded Cogency, an engineering research firm specialising in the development of imaging and data analysis software. His expertise lies in automated video surveillance, particle tracking and 3D shape characterisation. Mathew Price is the corresponding author and can be contacted at: mathew@cogency.co.za

Garry Morrison obtained a PhD degree in Laser Physics from the University of St Andrews in 1996. He then joined the De Beers Industrial Diamond Division (now Element 6), where he developed an interest in the wear and fracture properties of brittle materials. After moving to DebTech in 2001, his interests expanded to include particulate process optimisation, DEM simulation, 3D particle shape characterisation and particulate fracture.

This article has been cited by:

1. Lei Liu, Zhimin Zhao. 2013. A new approach for measurement of pitch, roll and yaw angles based on a circular feature. *Transactions of the Institute of Measurement and Control* **35**:3, 384-397. [CrossRef]